Progress In Electromagnetics Research B, Vol. 34, 225–245, 2011

INFLUENCE OF CONSTANT VALUES AND MOTOR PARAMETERS DEVIATIONS ON THE PERFORMANCE OF THE ADAPTIVE SLIDING-MODE OBSERVER IN A SENSORLESS INDUCTION MOTOR DRIVE

P. J. Costa Branco* **and J. Ferraz**

Technical University of Lisbon, Instituto Superior Técnico (IST), DEEC-Energia, Av. Rovisco Pais, Lisboa 1049-001, Portugal

Abstract—The adaptive sliding-mode observer has been widely used to estimate the rotor flux and rotor speed in inverter-fed sensorless induction motor drives. However, the technique requires setting *a priori* the sliding-mode observer constants and also knowledge of the induction motor parameters. This particular aspect can cause significant errors in the estimation of the rotor speed used in sensorless control schemes. Changes in the induction machine parameters due to temperature or different saturation levels will affect the dynamic operation of the observer despite its adaptive nature. In this context, a sensitivity study of the adaptive sliding-mode observer is presented and discussed in this paper. Various experiments are performed on a sensorless indirect vector-controlled induction motor drive under a variety of conditions to verify the observer robustness.

1. INTRODUCTION

Several applications of the simple adaptive sliding-mode observer [1] or its improvements for sensorless induction motor drives have been developed in the literature in the last years. References [2–18] resume some of the research proposed in the last years, together with other techniques as, for example, using high gain observers [19, 20]. However, the influence of the constants and motor parameters deviation on the adaptive observer performance has been little considered. It is in this context that this paper presents the constants and motor parameters sensitivity study and several experiments of the adaptive sliding-mode observer in a sensorless induction motor drive.

Received 16 August 2011, Accepted 10 September 2011, Scheduled 14 September 2011
* Corresponding author: Paulo José da Costa Branco (pbranco@ist.utl.pt).

2. INDUCTION MOTOR MODEL

The induction motor model with the stator currents and rotor flux as state variables can be written in the stationary-coordinate system by

$$\frac{d}{dt}\begin{bmatrix}\mathbf{i}_s\\ \boldsymbol{\psi}_r\end{bmatrix}=\mathbf{A}\begin{bmatrix}\mathbf{i}_s\\ \boldsymbol{\psi}_r\end{bmatrix}+\mathbf{B}\begin{bmatrix}\mathbf{u}_s\\ 0\end{bmatrix}, \tag{1}$$

where $\mathbf{i}_s$ corresponds to DQ components of stator currents, $\mathbf{u}_s$ is the vector of DQ components of stator voltages, and $\boldsymbol{\psi}_r$ is the vector of DQ components of rotor flux, all defined as

$$\mathbf{i}_s=\begin{bmatrix}i_{Ds}\\ i_{Qs}\end{bmatrix},\quad \mathbf{u}_s=\begin{bmatrix}u_{Ds}\\ u_{Qs}\end{bmatrix},\quad \boldsymbol{\psi}_r=\begin{bmatrix}\psi_{Dr}\\ \psi_{Qr}\end{bmatrix}. \tag{2}$$

Matrices $\mathbf{A}$ and $\mathbf{B}$ are given by

$$\mathbf{A}=\begin{bmatrix}\mathbf{A}_{11} & \mathbf{A}_{12}\\ \mathbf{A}_{21} & \mathbf{A}_{22}\end{bmatrix},\quad \mathbf{B}=\begin{bmatrix}\mathbf{B}_1\\ 0\end{bmatrix}, \tag{3}$$

where

$$\begin{aligned}&\mathbf{A}_{11}=-\eta\mathbf{I},\qquad \mathbf{A}_{12}=\beta\left(\tau_r^{-1}\mathbf{I}-p\omega\mathbf{J}\right),\\ &\mathbf{A}_{21}=\tau_r^{-1}M\mathbf{I},\quad \mathbf{A}_{22}=\tau_r^{-1}\mathbf{I}-p\omega\mathbf{J},\quad \mathbf{B}_1=\frac{1}{\sigma L_s}\mathbf{I}\end{aligned} \tag{4}$$

and

$$\begin{aligned}&\sigma=1-\frac{M^2}{L_sL_r},\ \beta=\frac{M}{\sigma L_sL_r},\quad \eta=\frac{M^2R_r+L_r^2R_s}{\sigma L_sL_r^2},\quad \tau_r=\frac{L_r}{R_r},\\ &\mathbf{I}=\begin{bmatrix}1 & 0\\ 0 & 1\end{bmatrix},\quad \mathbf{J}=\begin{bmatrix}0 & -1\\ 1 & 0\end{bmatrix},\end{aligned} \tag{5}$$

where M is the mutual inductance coefficient, L_s and L_r are respectively the stator and rotor inductance coefficients, R_s and R_r are respectively the stator and rotor phase resistances, ω being the motor speed, and p being the number of pole pairs. Using (2) to (5) in (1) yields

$$\frac{di_{Ds}}{dt}=(-\eta)\,i_{Ds}+\left(\beta\tau_r^{-1}\right)\psi_{Dr}+(\beta p\omega)\,\psi_{Qr}+\left(\frac{1}{\sigma L_s}\right)u_{Ds}, \tag{6a}$$

$$\frac{di_{Qs}}{dt}=(-\eta)\,i_{Qs}-(\beta p\omega)\,\psi_{Dr}+\left(\beta\tau_r^{-1}\right)\psi_{Qr}+\left(\frac{1}{\sigma L_s}\right)u_{Qs}, \tag{6b}$$

$$\frac{d\psi_{Dr}}{dt}=\left(\tau_r^{-1}M\right)i_{Ds}-\tau_r^{-1}\psi_{Dr}-(p\omega)\,\psi_{Qr}, \tag{6c}$$

$$\frac{d\psi_{Qr}}{dt}=\left(\tau_r^{-1}M\right)i_{Qs}+(p\omega)\,\psi_{Dr}-\tau_r^{-1}\psi_{Qr}, \tag{6d}$$

which is the induction motor model in DQ coordinates in stationary-coordinate system. The electromagnetic torque is given by

$$T_e = \frac{3}{2}\frac{pM}{L_r}\left(\psi_{Dr}\psi_{Qs} - \psi_{Qr}\psi_{Ds}\right). \tag{7}$$

3. THE ADAPTIVE SLIDING-MODE OBSERVER: REVIEW

3.1. Rotor Flux Estimation

The adaptive observer can be expressed by (8) where $\hat{\mathbf{x}}$ is the vector composed by DQ components of estimated stator current and estimated rotor flux (9), $\mathbf{K}$ is a gain matrix defined by (10) and (11). Currents $\hat{\imath}_{Ds}$ and $\hat{\imath}_{Qs}$ are estimated and compared with those ones measured to produce an error variable for the sliding observer estimate the rotor flux components and thus the rotor speed. This is why the sliding error variable is used to guide the observer.

$$\frac{d\hat{\mathbf{x}}}{dt} = \mathbf{A}\hat{\mathbf{x}}+\mathbf{B}\mathbf{u}_s+\mathbf{K}\,sgn\left(\hat{\mathbf{I}}_s-\mathbf{i}_s\right) \tag{8}$$

$$\hat{\mathbf{x}} = \begin{bmatrix} \hat{\mathbf{I}}_s \\ \hat{\boldsymbol{\psi}}_r \end{bmatrix} = \begin{bmatrix} \hat{\imath}_{Ds} \\ \hat{\imath}_{Qs} \\ \hat{\psi}_{Dr} \\ \hat{\psi}_{Qr} \end{bmatrix} \tag{9}$$

$$\mathbf{K} = \begin{bmatrix} \mathbf{K}_1 \\ -\mathbf{L}\mathbf{K}_1 \end{bmatrix} \tag{10}$$

$$\mathbf{K}_1 = \begin{bmatrix} -k_1 & 0 \\ 0 & -k_2 \end{bmatrix} \mathbf{L} = \begin{bmatrix} l_{11} & l_{12} \\ l_{21} & l_{22} \end{bmatrix} \tag{11}$$

Developing (8), it is written as in (12).

$$\frac{d}{dt}\hat{\mathbf{I}}_s = \mathbf{A}_{11}\hat{\mathbf{I}}_s+\mathbf{A}_{12}\hat{\boldsymbol{\psi}}_r+\mathbf{B}_1\mathbf{u}_s+\mathbf{K}_1 sgn\left(\hat{\mathbf{I}}_s-\mathbf{i}_s\right) \tag{12a}$$

$$\frac{d\hat{\boldsymbol{\psi}}_r}{dt} = \mathbf{A}_{21}\hat{\mathbf{I}}_s + \mathbf{A}_{22}\hat{\boldsymbol{\psi}}_r - \mathbf{L}\mathbf{K}_1 sgn\left(\hat{\mathbf{I}}_s - \mathbf{i}_s\right) \tag{12b}$$

The matrix $\mathbf{K}_1$ values are set by trial-and-error to optimize the observer performance. To obtain the coefficients of matrix $\mathbf{L}$, the following expressions are defined [20]:

$$\begin{aligned} x &= (q-1)\,\varepsilon + \frac{\gamma}{\tau_r \varepsilon}, \\ y &= \frac{\gamma\omega}{\varepsilon}, \end{aligned} \tag{13}$$

with q and γ being constants assigned experimentally with ε defined as:

$$\varepsilon = \frac{\sigma L_s L_r}{M}. \tag{14}$$

The matrix $\mathbf{L}$ is thus calculated as in (15).

$$\begin{aligned} l_{11} &= -x \\ l_{12} &= y \\ l_{21} &= -y \\ l_{22} &= -x \end{aligned} \tag{15}$$

Expanding vectors $\hat{\mathbf{I}}_s = \left[\hat{\imath}_{Ds}, \hat{\imath}_{Qs}\right]^T$ and $\hat{\boldsymbol{\psi}}_r = \left[\hat{\psi}_{Dr}, \hat{\psi}_{Qr}\right]^T$, as well as the matrices $\mathbf{A}_{11}$, $\mathbf{A}_{12}$, $\mathbf{A}_{21}$, $\mathbf{A}_{22}$, $\mathbf{K}_1$, $\mathbf{LK}_1$ gives the set of differential equations for stator currents and rotor flux indicated in (16). The system has as input variables the voltages u_{Ds} and u_{Qs}, currents i_{Ds} and i_{Qs} and the rotor speed measured ω or estimated $\hat{\omega}$. The variables to be estimated are the components of the stator current in stationary reference frame, $\hat{\imath}_{Ds}$ and $\hat{\imath}_{Qs}$ and the rotor flux components in the same reference, $\hat{\psi}_{Dr}$ and $\hat{\psi}_{Qr}$

$$\frac{d\hat{\imath}_{Ds}}{dt} = -\eta\hat{\imath}_{Ds} + \frac{\beta}{\tau_r}\hat{\psi}_{Dr} + \beta p\omega\hat{\psi}_{Qr} + \frac{1}{\sigma L_s}u_{Ds} - k_1 sgn(\hat{\imath}_{Ds} - i_{Ds}) \tag{16a}$$

$$\frac{d\hat{\imath}_{Qs}}{dt} = -\eta\hat{\imath}_{Qs} - \beta p\omega\hat{\psi}_{Dr} + \frac{\beta}{\tau_r}\hat{\psi}_{Qr} + \frac{1}{\sigma L_s}u_{Qs} - k_2 sgn(\hat{\imath}_{Qs} - i_{Qs}) \tag{16b}$$

$$\begin{aligned} \frac{d\hat{\psi}_{Dr}}{dt} = {} & \frac{M}{\tau_r}\hat{\imath}_{Ds} - \frac{1}{\tau_r}\hat{\psi}_{Dr} - p\omega\hat{\psi}_{Qr} + l_{11}k_1 sgn\left(\hat{\imath}_{Ds} - i_{Ds}\right) \\ & + l_{12}k_2 sgn(\hat{\imath}_{Qs} - i_{Qs}) \end{aligned} \tag{16c}$$

$$\begin{aligned} \frac{d\hat{\psi}_{Qr}}{dt} = {} & \frac{M}{\tau_r}\hat{\imath}_{Qs} + p\omega\hat{\psi}_{Dr} - \frac{1}{\tau_r}\hat{\psi}_{Qr} + l_{21}k_1 sgn\left(\hat{\imath}_{Ds} - i_{Ds}\right) \\ & + l_{22}k_2 sgn(\hat{\imath}_{Qs} - i_{Qs}) \end{aligned} \tag{16d}$$

3.2. Rotor Speed Estimation

Consider the error Equation (17) and the Lyapunov function (18) where $\mathbf{e}_{\boldsymbol{\psi}}$ is the matrix $[e_{D\psi}\, e_{Q\psi}]^{\mathrm{T}}$ (Appendix A) and function W must be such as to ensure convergence of the rotor speed estimation according to the theory of Lyapunov stability.

$$\frac{d\mathbf{e}_{\boldsymbol{\psi}}}{dt} = -\boldsymbol{\Lambda}\mathbf{K_1} sgn\left(\hat{\mathbf{I}}_{\mathbf{s}} - \mathbf{i}_{\mathbf{s}}\right) \tag{17}$$

$$\mathbf{V} = \mathbf{e}_{\boldsymbol{\psi}}^{\mathbf{T}}\mathbf{e}_{\boldsymbol{\psi}} + W \tag{18}$$

The derivative of Lyapunov function (18) is given by

$$\frac{d}{dt}\mathbf{V} = \frac{d}{dt}\left(\mathbf{e}_{\boldsymbol{\psi}}^{\mathbf{T}}\right)\mathbf{e}_{\boldsymbol{\psi}} + \mathbf{e}_{\boldsymbol{\psi}}^{\mathbf{T}}\frac{d}{dt}\left(\mathbf{e}_{\boldsymbol{\psi}}\right) + \frac{dW}{dt}. \tag{19}$$

Defining a variable $\mathbf{z}$ as in (20), substituting Equations (17) and (20) in (19), and after performing the derivatives the result is given by (21).

$$\mathbf{z} = -\mathbf{K_1} sgn\left(\hat{\mathbf{I}}_{\mathbf{s}} - \mathbf{i}_{\mathbf{s}}\right) \tag{20}$$

$$\frac{d}{dt}\mathbf{V} = \mathbf{z}^{\mathbf{T}}\boldsymbol{\Lambda}^{\mathbf{T}}\mathbf{A}_{\mathbf{12}}^{-\mathbf{1}}\mathbf{z} + \mathbf{z}^{\mathbf{T}}\boldsymbol{\Lambda}^{\mathbf{T}}\mathbf{A}_{\mathbf{12}}^{-\mathbf{1}}\frac{\Delta\omega_r}{\varepsilon}\mathbf{J}\boldsymbol{\psi}_{\mathbf{r}} + \frac{dW}{dt} \tag{21}$$

The derivative of Lyapunov function $\mathbf{V}$ with respect to time can be expressed as:

$$\frac{d}{dt}\mathbf{V} = \frac{d}{dt}\mathbf{V_1} + \frac{d}{dt}\mathbf{V_2} \tag{22}$$

Therefore, equating expressions (21) and (22) gives

$$\begin{cases} \frac{d}{dt}\mathbf{V_1} = \mathbf{z}^{\mathbf{T}}\boldsymbol{\Lambda}^{\mathbf{T}}\mathbf{A}_{\mathbf{12}}^{-\mathbf{1}}\mathbf{z}, \\ \frac{d}{dt}\mathbf{V_2} = \mathbf{z}^{\mathbf{T}}\boldsymbol{\Lambda}^{\mathbf{T}}\mathbf{A}_{\mathbf{12}}^{-\mathbf{1}}\frac{\Delta\omega}{\varepsilon}\mathbf{J}\boldsymbol{\psi}_{\mathbf{r}} + \frac{dW}{dt}. \end{cases} \tag{23}$$

According to the theory of Lyapunov stability, to be ensured stability, equation (22) must be negative definite. For that, conditions (24) and (25) must be imposed

$$\frac{d}{dt}\mathbf{V_1} < 0 \tag{24}$$

$$\frac{d}{dt}\mathbf{V_2} = 0 \tag{25}$$

In order to achieve the first condition (24), we must establish the equality of (26) where constant γ must have a positive value. Using (26) provided (24) results in (27). This equation will always be negative definite since it is always imposed positive values for γ

$$\boldsymbol{\Lambda}^{\mathbf{T}} = -\gamma\mathbf{A_{12}}, \quad \gamma > 0 \tag{26}$$

$$\frac{d}{dt}\mathbf{V_1} = -\mathbf{z}^{\mathbf{T}}\gamma\mathbf{z} \tag{27}$$

Substituting (26) in the second equation of (23), gives

$$\frac{d}{dt}\mathbf{V_2} = -\boldsymbol{\gamma}\mathbf{z}^{\mathbf{T}}\frac{\Delta\omega}{\varepsilon}\mathbf{J}\boldsymbol{\psi}_{\mathbf{r}} + \frac{dW}{dt}. \tag{28}$$

Applying the condition (25) in (28) we obtain the result expressed by (29).

$$\frac{dW}{dt} = \gamma\mathbf{z}^{\mathrm{T}}\frac{\Delta\omega}{\varepsilon}\mathbf{J}\boldsymbol{\psi}_{\mathbf{r}} \tag{29}$$

Thus, from (29), function W can be chosen equal to (30), in which parameter μ should also have a positive value

$$W = \frac{\Delta\omega}{2\mu\varepsilon}, \quad \mu > 0 \tag{30}$$

Deriving (30) with respect to time, yields

$$\frac{dW}{dt} = \frac{2\Delta\omega}{2\mu\varepsilon}\frac{d\omega}{dt} \tag{31}$$

Developing (29) using (20), we obtain

$$\frac{dW}{dt} = \gamma\left[k_{11}sgn\left(\hat{\imath}_{Ds} - i_{Ds}\right) \quad k_{22}sgn\left(\hat{\imath}_{Qs} - i_{Qs}\right)\right]\frac{\Delta\omega}{\varepsilon}\begin{bmatrix}0 & -1\\ 1 & 0\end{bmatrix}\begin{bmatrix}\hat{\psi}_{Dr}\\ \hat{\psi}_{Qr}\end{bmatrix}. \tag{32}$$

Now rewriting (32), gives

$$\frac{dW}{dt} = \gamma\frac{\Delta\omega}{\varepsilon}\left[k_{11_1}sgn\left(\hat{\imath}_{Ds} - i_{Qs}\right)\hat{\psi}_{Qr} - k_{22_2}sgn\left(\hat{\imath}_{Qs} - i_{Qs}\right)\hat{\psi}_{Dr}\right]. \tag{33}$$

Finally, equalizing (31) and (33), we obtain the equation of the rotor speed estimator defined by

$$\frac{d\hat{\omega}}{dt} = \mu\gamma\left[k_{11}sgn\left(\hat{\imath}_{Ds} - i_{Ds}\right)\hat{\psi}_{Qr} - k_{22}sgn(\hat{\imath}_{Qs} - i_{Qs})\hat{\psi}_{Dr}\right] \tag{34}$$

According to Equations (26) and (30), positive parameters μ and γ in (34) have to be chosen in order to optimize the performance of the rotor speed estimator. At this time, there is no way to attribute their value using an analytical equation. Therefore, their values must be attributed by trial-and-error, being tuned for a stable and fast sliding observer. Their influence is distinct because, while parameter μ only directly influences the progress of the estimated speed, parameter γ directly affects not only the estimated speed, but also the stator current and rotor flux estimates, as parameter γ is included in matrix $\mathbf{L}$. Notice that, in general, the increase of these parameters results in a faster transient response of the observer. However, this increase reduces the robustness of the observer when in stationary regime, showing some oscillations in the estimated speed as will be discussed in the next section.

4. IMPLEMENTATION OF THE ADAPTIVE SLIDING-MODE OBSERVER: EXPERIMENTAL RESULTS

The experimental setup used for our sensitivity study is shown in Fig. 1(a). It consists in an electrical drive system with a 370 W cage

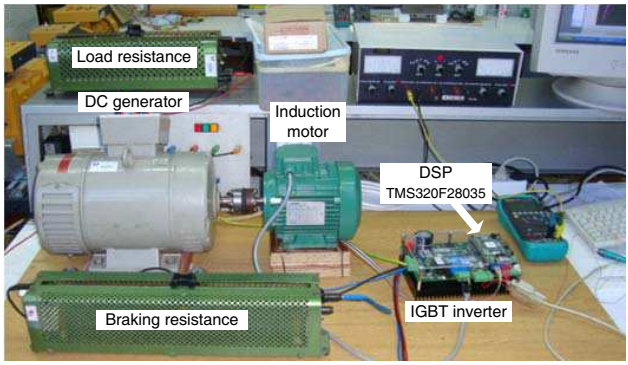

(a)

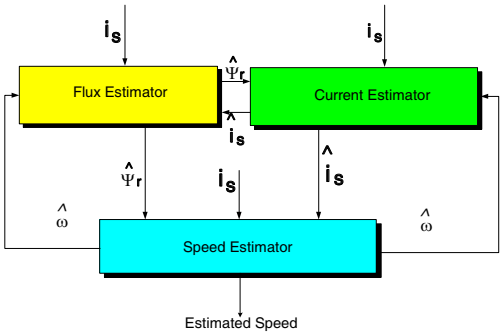

(b)

Figure 1. (a) DSP-based induction motor drive system used to verify the parameter sensitivity of the modified adaptive sliding-mode observer. The experimental setup consists in an induction motor, an IGBT inverter, a DC generator used as loading machine, and a DSP (TMS320F28035) board. (b) Block diagram of the sliding-mode observer implemented in the DSP.

induction motor (parameters listed in Table 1), an IGBT inverter controlled by a Texas Instruments DSP TMS320F28035 using a SVPWM (Space Vector PWM) algorithm, and a DC generator used as motor load. The braking resistance is used by the induction motor drive when braking. The IGBT inverter inverts the electric power direction and this is dissipated in the braking resistor to decrease the motor speed. The induction motor is equipped with a speed sensor (incremental encoder) and also has two current sensors (Hall Effect sensors). Fig. 1(b) shows in a block diagram the observer structure, which was implemented in the DSP.

Table 1. Parameters of the 370 W one-pole Pair 50-Hz induction motor.

Rated power	370 W
Rated voltage	400 V
Rated torque	1.3 Nm
Rated speed	2820 rpm
Rated current	1.7 A
Magnetizing inductance M	1.46 H
Stator inductance L_s	1.48 H
Rotor inductance L_r	1.48 H
Stator resistance R_s	16.1 Ω
Rotor resistance R_r	24.6 Ω
Total moment of inertia	0.00035 kgm

The drive system topology consists in an indirect vector speed control of the induction motor. Generally, this control works best for drives that use a speed sensor to measure the rotor speed. In sensorless mode, the speed information is not available by direct measurement and in our case it must be estimated by the modified sliding-mode observer. The scheme of the implemented sensorless induction motor control used in this research is shown in Fig. 2. The controller and observer were all programmed in the DSP board together with the SVPWM current control for the IGBT inverter. The influence of constants values and the motor parameters deviation in the adaptive observer performance was extensively tested using this experimental setup.

4.1. Stator Currents and Rotor Flux Estimation

In this section, results concerning the estimation of the components of the stator currents ($\hat{\imath}_{Ds}$, $\hat{\imath}_{Qs}$) and rotor flux ($\hat{\psi}_{Dr}$, $\hat{\psi}_{Qr}$) are presented both in steady-state and in transient regime. In this experiment, it was not used any speed sensor with the induction motor drive. The observer uses the reference voltages u_{Ds} and u_{Qs}, employed in the indirect field oriented control, and uses the currents i_{Ds} and i_{Qs} obtained from the transformation abc/DQ of the measured stator currents i_a and i_b.

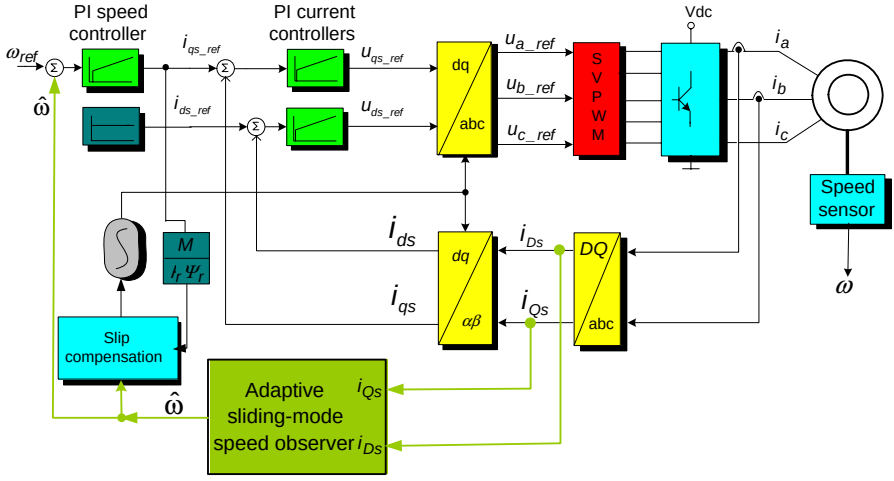

Figure 2. Block diagram of sensorless indirect vector speed control of the induction motor.

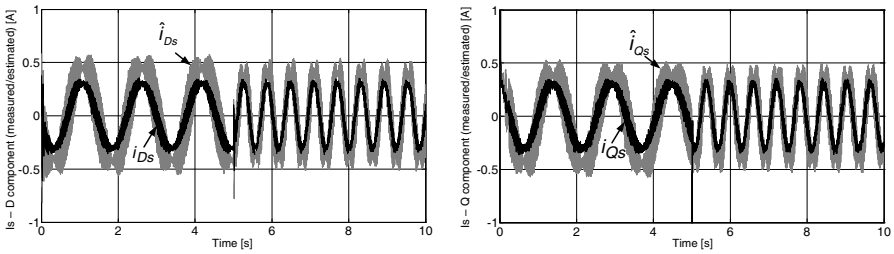

(a) (b)

Figure 3. (a) The D components of the measured i_{Ds} and estimated $\hat{i}_{Ds}$ stator currents. (b) The Q components of the measured i_{Qs} and estimated $\hat{i}_{Qs}$ stator currents.

4.1.1. Stator Currents

Figure 3(a) shows the estimated current $\hat{i}_{Ds}$. Fig. 3(b) shows the estimated current $\hat{i}_{Qs}$. As can be verified in Figs. 3(a) and 3(b) the estimated currents using the observer follow the measured one with low significant error. All results were obtained in low speed values, with a reference speed of 90 rpm following to 30 rpm.

Figure 4(a) shows the measured current i_{Ds} and the estimated current $\hat{i}_{Ds}$ when the rotor speed is equal to 450 rpm. The current components i_{Qs} and $\hat{i}_{Qs}$ are not shown since they have similar trends.

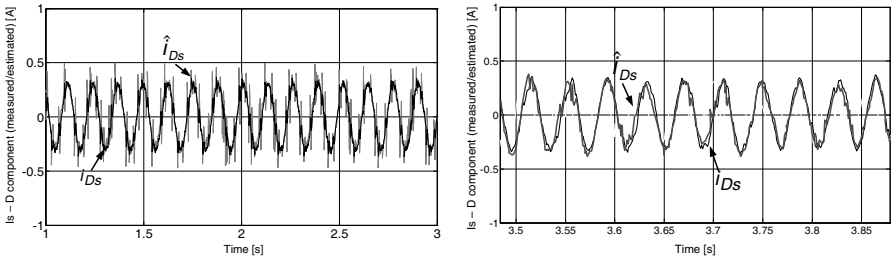

Figure 4. Measured current i_{Ds} and estimated current $\hat{\imath}_{Ds}$ for a (a) rotor speed equal to 450 rpm and (b) for a speed equal to 150 rpm.

At last Fig. 4(b) shows for a higher rotor speed equal to 1500 rpm the measured i_{Ds} and the estimated current $\hat{\imath}_{Ds}$. Both results show the good performance of the implemented observer in a wide speed range.

4.1.2. Rotor Flux

The experimental results regarding the estimation of rotor flux DQ components were obtained for a low speed value of 30 rpm (Fig. 5(a)), an average speed of 450 rpm (Fig. 5(b)), and a high speed of 1500 rpm (Fig. 5(c)). We verify in all three results that the DQ estimated rotor flux components have equal amplitudes and a dephasing angle of 90° as expected. Furthermore, each component has a frequency related to the rotor speed.

4.2. Performance of the Observer When in the Sensorless Indirect Field Oriented Controller

This section presents the performance of the indirect field oriented control without using the speed sensor, but using the adaptive observer and its estimated rotor speed. Results were obtained for various speed reference profiles. Because the evolution of the real speed was very near to the estimated one, figures only show the estimated rotor speed.

Figure 6(a) shows the speed reference ω_{ref} which is characterized by a ramp speed from 0 to +750 rpm in 5 seconds, and then for a constant speed equal to +750 rpm. This figure also presents the evolution of the estimated speed $\hat{\omega}$. From the results obtained, it appears that for the first 2 seconds the speed controller works to bring the estimated speed to the reference one. Here is also found that the delay was due to the convergence process inherent to the speed observer. In the following instants, the estimated speed follows the

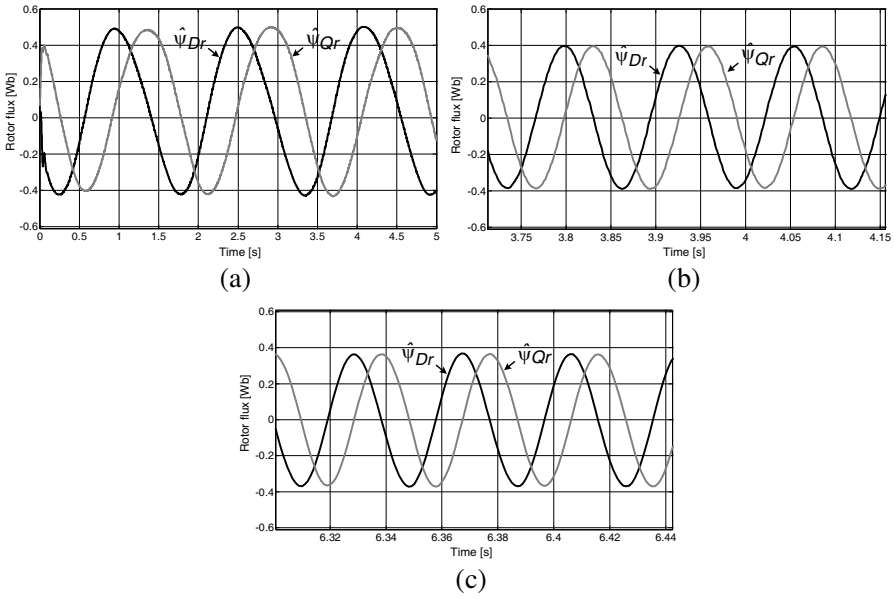

Figure 5. Rotor flux estimated components $\hat{\psi}_{Dr}$ and $\hat{\psi}_{Qr}$ for a speed equal to (a) 30 rpm, (b) 450 rpm, and (c) 1500 rpm, using the modified observer.

speed reference with very good approximation, showing an average error of about +3% to reach the steadystate. Follow, the average error stays significantly lower in +1%.

A second test was carried out but being opposite to that anterior. It uses now a reference speed ramp with a negative slope and a steady-state speed equal to −750 rpm, as shown in Fig. 6(b). The evolution of the estimated speed is similar to the anterior results in Fig. 6(a).

Figure 6(c) shows the results obtained when a pyramid type reference is applied to the speed controller. After the initial seconds that are associated with the control system and the observer convergence, the error between the reference and estimated speed decreased to a value around 2%. This confirms the good performance of the sensorless speed control implemented

An interesting test was performed which required a motor acceleration from 0 to −750 rpm, maintaining this speed during 2 seconds, and finally braking to 0 rpm. Fig. 6(d) shows the speed reference signal and the evolution obtained by the estimated speed. During acceleration and deceleration, the error shows an average value of +3%. However, during the two seconds of steady state, the

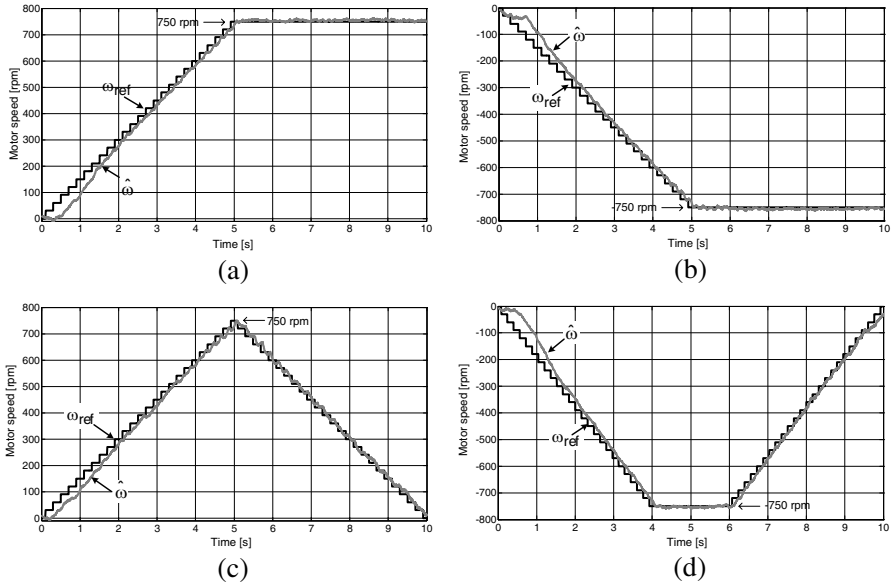

Figure 6. Indirect field oriented control without speed sensor but using the speed estimated by the modified observer. (a) Speed reference ω_{ref} in ramp with positive slope and the estimated speed $\hat{\omega}$. (b) Speed reference ω_{ref} in ramp with negative slope and the estimated speed $\hat{\omega}$. (c) Speed reference ω_{ref} in pyramid form and estimated speed $\hat{\omega}$. (d) Reference speed ω_{ref} accelerates from 0 rpm to -750 rpm, maintained for 2 seconds and then slows up again at 0 rpm, and estimated speed $\hat{\omega}$.

error drops significantly to a mean value less than +1%, showing the excellent performance of indirect field-oriented speed sensorless.

5. PARAMETER SENSITIVITY OF THE ADAPTIVE OBSERVER

In order to identify the adaptive sliding-mode observer parameters that have the most impact on its performance, a parameter sensitivity analysis was performed. Experimental results in this section analyze the sensitivity to the observer constants and also motor parameters variation.

5.1. Observer Sensitivity Under its Constants

The set of parameters of the observer, whose values were assigned, is listed in Table 2. Since most parameters are assigned by trial-and-error, it is important to check the sensitivity of each parameter in order to determine which ones are the most significant and also defining what should be the first parameter to have assigned a value.

Figure 7(a) shows the results for parameter μ. Note that this parameter directly influences the evolution of estimated speed $\hat{\omega}$, as can be seen from Eq. (34). The results in Fig. 7(a) show that this parameter affects the convergence time of the estimated speed to the measured one. Taking as reference the results obtained with $\Delta\mu = 0$, it appears that when parameter μ has its value increased by 50% ($\Delta\mu = +50\%$) the evolution of estimated speed to the measured one becomes more fast. However, we observe that in steady-state, the estimated speed started to show significant fluctuations around the value of measured speed. In the opposite condition, where parameter μ had its value reduced by 50% ($\Delta\mu = -50\%$), the convergence time became greater, as shown in Fig. 7(a). However, the estimated speed started to show a steadystate without significant fluctuations

Figure 7(b) shows the variation of parameter γ, which is also directly used in Eq. (34) to obtain the estimated speed. The results are similar to those presented with parameter μ, also showing the great sensitivity of the estimator for parameter γ.

The last parameters tested were k_1, k_2, included in the diagonal

Table 2. Constants used in the adaptive observer.

k_1	0.0216
k_2	0.0216
l_{11}	-0.48537
l_{22}	-0.48537
l_{12}	0.0459
l_{21}	-0.0459
μ	3.396×10^6
γ	0.0019
ε	1.45997 H
q	0.65

matrix equations $\mathbf{K_1}$ and $\mathbf{K_{1m}}$ present in observer Equation (12). Fig. 7(c) shows the results when the parameters change. For a variation of -50% ($\Delta k_1 = \Delta k_2 = -50\%$), the observer dynamics becomes more slow in its convergence to the measured speed, with a small oscillatory behavior in its steady-state after reaching the measured speed. For an opposite variation of $+50\%$ ($\Delta k_1 = \Delta k_{1m} = \Delta k_2 = \Delta k_{2m} = +50\%$), the observer dynamics becomes faster, acquiring however a significant oscillatory behavior after reaching the measured speed, as shown in Fig. 7(c).

For parameters l_{11}, l_{22}, l_{12}, l_{21} of matrix $\mathbf{L}$ in (12), which are include in the equations for estimating the rotor flux, and parameter q, the tests performed with both positive and negative variations of these parameters led to the conclusion that a variation of the same does not significantly affect the dynamics of the observer. For this reason the results were not included.

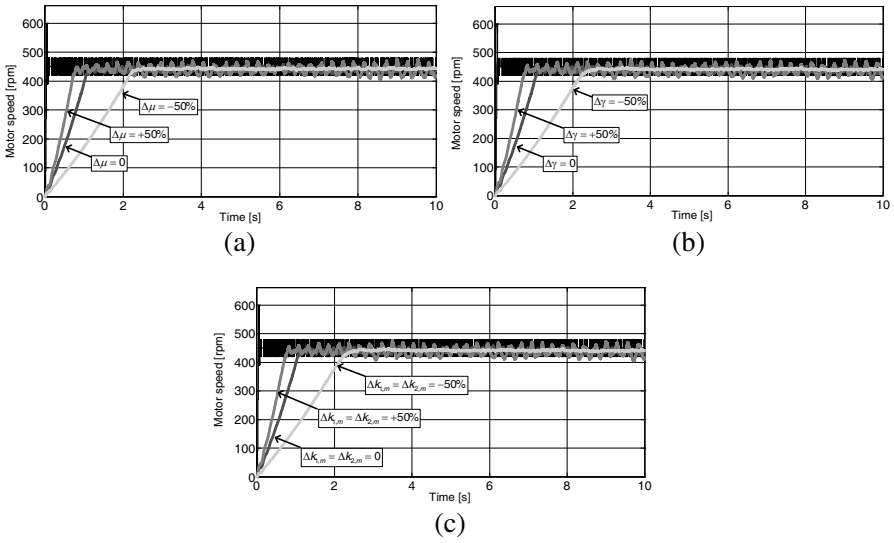

Figure 7. (a) Parameter μ. The measured speed ω (black) and estimated $\hat{\omega}$ (color with different levels of gray) for the following changes in the value of μ $\Delta\mu = 0$, $\Delta\mu = +50\%$, and $\Delta\mu = -50\%$. (b) Parameter γ. The measured speed ω (black) and estimated $\hat{\omega}$ (color with different levels of gray) for the following changes in the value of γ $\Delta\gamma = 0$, $\Delta\gamma = +50\%$, e $\Delta\gamma = -50\%$. (c) Parameters k_{11}, and k_{22}, from matrix equations $\mathbf{K}_1$. The measured speed ω (black) and estimated $\hat{\omega}$ (color with different levels of gray) for the following changes: ($\Delta k_{11} = \Delta k_{22} = +50\%$).

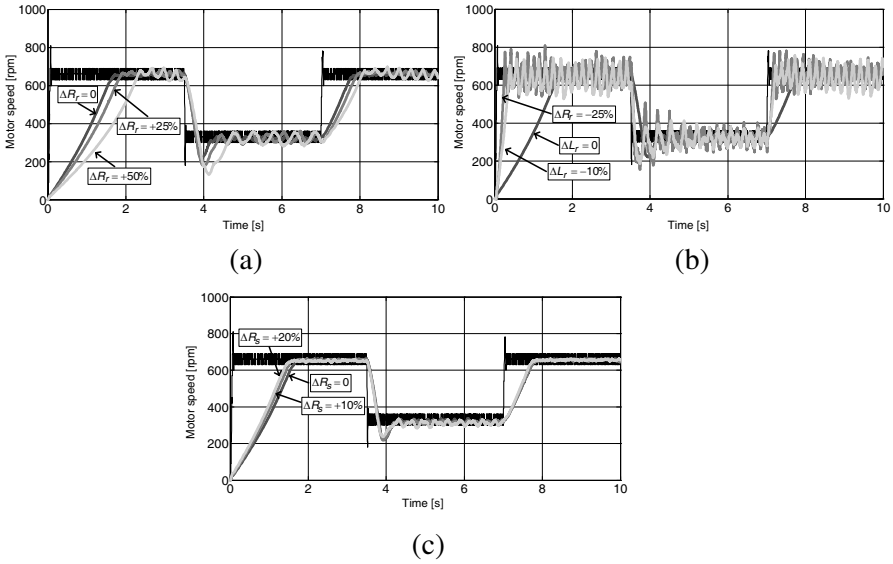

Figure 8. (a) Rotor resistance R_r variation. The measured speed ω (black) and estimated $\hat{\omega}$ (color with different gray levels) for the following R_r increase: $\Delta R_r = 0$, $\Delta R_r = +25\%$, e $\Delta R_r = +50\%$. (b) Induction rotor coefficient L_r variation. The measured speed ω (black) and estimated $\hat{\omega}$ (color with different gray levels) for the following L_r decrease: $\Delta L_r = 0$, $\Delta L_r = -10\%$, e $\Delta L_r = -25\%$. (c) Rotor resistance R_s variation. The measured speed ω (black) and estimated $\hat{\omega}$ (color with different gray levels) for the following R_s increase: $\Delta R_s = 0$, $\Delta R_s = +10\%$, e $\Delta R_s = +20\%$.

5.2. Observer Sensitivity Under Motor Parameters Variation

This section evaluates the performance of the observer under changes in the induction motor parameters. Experimental results are shown for variations in the values of rotor resistance R_r, rotor inductance L_r, and the stator resistance R_s.

For rotor resistance, its variation was only contemplated for an increase of its value caused by a possible temperature augmentation. Fig. 8(a) shows the experimental curves of the estimated speed. The results show that as the rotor resistance increases, the convergence of the observer to measured speed becomes slower. Moreover, in steady-state, the estimator behaves increasingly oscillatory for a rotor resistance increase.

To study the behavior of the observer for an L_r variation, it was considered only a reduction of its value since it is associated with the

motor operating with magnetic saturation. There were established two decreases in this parameter: -10% and -25% of its initial value. The curves of the estimated speed in Fig. 8(b) show not only a considerable decrease in the convergence time of the observer for decreasing of the rotor induction coefficient, but also an excessively oscillatory behavior around the measured speed.

Next, we analyzed the observer sensitivity when there was an increase in the value of the stator resistance R_s. We considered two increases: $+10\%$ and $+20\%$. Fig. 8(c) shows the results. In general, one can say that the observer is insensitive to a stator resistance variation, either in their time of convergence as in steady-state.

6. CONCLUSION

Parameter variations in an induction motor drive under sensorless operation based on the adaptive sliding-mode observer induce flux deviations from the command value and oscillations during dynamic operation. More significant is the observer sensitivity to the values attributed by the user to the constants used by the observer. Based on the experimental verification of the observer parameter sensitivity, automatic tuning methods can be applied to change the observer constants and adapt it to different speed and also acceleration levels.

APPENDIX A.

Defining $\Delta\omega = \hat{\omega} - \omega$, and rewriting it as $\hat{\omega} = \omega + \Delta\omega$, it is easily verified that $\hat{\mathbf{A}} = \mathbf{A} + \mathbf{\Delta A}$, which $\mathbf{\Delta A}$ arises due to the difference between estimated and measured speed. This new matrix is then constructed as $\mathbf{\Delta A} = \hat{\mathbf{A}} - \mathbf{A}$. Observing the elements of $\mathbf{A}$, matrices $\mathbf{A_{11}}$ and $\mathbf{A_{21}}$ do not depend on ω and, since its elements are all constants, we conclude that these are equal to $\hat{\mathbf{A}}_{\mathbf{11}}$ and $\hat{\mathbf{A}}_{\mathbf{21}}$, respectively, since $\mathbf{\Delta A_{11}} = \mathbf{\Delta A_{21}} = 0$.

Matrix $\hat{\mathbf{A}}_{\mathbf{12}}$ is decomposed as:

$$\begin{aligned}\hat{\mathbf{A}}_{\mathbf{12}} &= \beta \begin{bmatrix} \tau_r^{-1} & p\hat{\omega} \\ -p\hat{\omega} & \tau_r^{-1} \end{bmatrix} = \beta \begin{bmatrix} \tau_r^{-1} & p(\omega + \Delta\omega) \\ -p(\omega + \Delta\omega) & \tau_r^{-1} \end{bmatrix} \\ &= \beta \begin{bmatrix} \tau_r^{-1} & p\omega \\ -p\omega & \tau_r^{-1} \end{bmatrix} - \beta \begin{bmatrix} 0 & -p\Delta\omega \\ p\Delta\omega & 0 \end{bmatrix}, \end{aligned} \tag{A1}$$

concluding that, as expected, $\hat{\mathbf{A}}_{\mathbf{12}} = \mathbf{A_{12}} + \mathbf{\Delta A_{12}}$, where

$$\mathbf{\Delta A_{12}} = -\beta \begin{bmatrix} 0 & -p\Delta\omega \\ p\Delta\omega & 0 \end{bmatrix} = -\beta p \Delta\omega \mathbf{J}. \tag{A2}$$

Matrix $\hat{\mathbf{A}}_{\mathbf{22}}$ can be also decomposed as

$$\begin{aligned}\hat{A}_{\mathbf{22}} &= \begin{bmatrix} -\tau_r^{-1} & p\hat{\omega} \\ -p\hat{\omega} & -\tau_r^{-1} \end{bmatrix} = \begin{bmatrix} -\tau_r^{-1} & p(\omega+\Delta\omega) \\ -p\,(\omega+\Delta\omega) & -\tau_r^{-1} \end{bmatrix} \\ &= \begin{bmatrix} -\tau_r^{-1} & p\omega \\ -p\omega & -\tau_r^{-1} \end{bmatrix} + \begin{bmatrix} 0 & p\Delta\omega \\ -p\Delta\omega & 0 \end{bmatrix}, \end{aligned} \tag{A3}$$

where $\hat{\mathbf{A}}_{\mathbf{22}} = \mathbf{A_{22}} + \mathbf{\Delta A_{22}}$ and thus $\mathbf{\Delta A_{22}}$ yields

$$\mathbf{\Delta A_{22}} = \begin{bmatrix} 0 & p\Delta\omega \\ -p\Delta\omega & 0 \end{bmatrix} = -p\Delta\omega\mathbf{J} \tag{A4}$$

At last, the matrix $\mathbf{\Delta A}$ becomes

$$\begin{aligned}\mathbf{\Delta A} &= \begin{bmatrix} \mathbf{\Delta A_{11}} & \mathbf{\Delta A_{12}} \\ \mathbf{\Delta A_{21}} & \mathbf{\Delta A_{22}} \end{bmatrix} = \begin{bmatrix} 0 & -\beta p\Delta\omega\mathbf{J} \\ 0 & -p\Delta\omega\mathbf{J} \end{bmatrix} \\ &= \begin{bmatrix} 0 & 0 & 0 & \beta p\Delta\omega \\ 0 & 0 & -\beta p\Delta\omega & 0 \\ 0 & 0 & 0 & p\Delta\omega \\ 0 & 0 & -p\Delta\omega & 0 \end{bmatrix} \end{aligned} \tag{A5}$$

Subtracting (6) from (12) results in

$$\frac{d}{dt}\hat{\mathbf{I}}_{\mathbf{s}} - \frac{d}{dt}\mathbf{i_s} = \mathbf{A_{11}}\left(\hat{\mathbf{I}}_{\mathbf{s}} - \mathbf{i_s}\right) + \hat{A}_{\mathbf{12}}\hat{\psi}_{\mathbf{r}} - \mathbf{A_{12}}\boldsymbol{\psi}_{\mathbf{r}} + \mathbf{K_1}sgn\left(\hat{\mathbf{I}}_{\mathbf{s}} - \mathbf{i_s}\right), \tag{A6}$$

$$\frac{d}{dt}\hat{\psi}_{\mathbf{r}} - \frac{d}{dt}\boldsymbol{\psi}_{\mathbf{r}} = \mathbf{A_{21}}\left(\hat{\mathbf{I}}_{\mathbf{s}} - \mathbf{i_s}\right) + \hat{A}_{\mathbf{22}}\hat{\psi}_{\mathbf{r}} - \mathbf{A_{22}}\boldsymbol{\psi}_{\mathbf{r}} + \mathbf{K_2}sgn\left(\hat{\mathbf{I}}_{\mathbf{s}} - \mathbf{i_s}\right). \tag{A7}$$

Defining the stator current and rotor flux errors as

$$\mathbf{e_i} = \hat{\mathbf{I}}_{\mathbf{s}} - \mathbf{i_s} \tag{A8}$$

$$\mathbf{e}_{\boldsymbol{\psi}} = \hat{\boldsymbol{\psi}}_{\mathbf{r}} - \boldsymbol{\psi}_{\mathbf{r}} \tag{A9}$$

and using them in (A6) and (A7), results in the following derivative error equations:

$$\frac{d}{dt}\mathbf{e_i} = \mathbf{A_{11}}\mathbf{e_i} + \mathbf{A_{12}}\mathbf{e}_{\boldsymbol{\psi}} + \mathbf{\Delta A_{11}}\hat{\mathbf{I}}_{\mathbf{s}} + \mathbf{\Delta A_{12}}\hat{\boldsymbol{\psi}}_{\mathbf{r}} + \mathbf{K_1}sgn\left(\hat{\mathbf{I}}_{\mathbf{s}} - \mathbf{i_s}\right), \tag{A10}$$

$$\frac{d}{dt}\mathbf{e}_{\boldsymbol{\psi}} = \mathbf{A_{21}}\mathbf{e_i} + \hat{A}_{\mathbf{22}}\hat{\boldsymbol{\psi}}_{\mathbf{r}} - \mathbf{A_{22}}\boldsymbol{\psi}_{\mathbf{r}} + \mathbf{K_2}sgn\left(\hat{\mathbf{I}}_{\mathbf{s}} - \mathbf{i_s}\right). \tag{A11}$$

To implement the sliding-mode dynamics, we have the conditions in (31).

$$\mathbf{e_i} = \frac{d}{dt}\mathbf{e_i} = 0 \tag{A12}$$

Using this condition in (A10) and (A11), results in

$$0 = \mathbf{A_{12}}\mathbf{e}_{\boldsymbol{\psi}} + \mathbf{\Delta A_{11}}\hat{\mathbf{I}}_{\mathbf{s}} + \mathbf{\Delta A_{12}}\hat{\boldsymbol{\psi}}_{\mathbf{r}} + \mathbf{K_1}sgn\left(\hat{\mathbf{I}}_{\mathbf{s}} - \mathbf{i_s}\right) \tag{A13}$$

$$\frac{d}{dt}\mathbf{e}_{\boldsymbol{\psi}} = \mathbf{A_{22}}\mathbf{e}_{\boldsymbol{\psi}} + \mathbf{\Delta A_{21}}\hat{\mathbf{I}}_{\mathbf{s}} + \mathbf{\Delta A_{22}}\hat{\boldsymbol{\psi}}_{\mathbf{r}} + \mathbf{K_2}sgn\left(\hat{\mathbf{I}}_{\mathbf{s}} - \mathbf{i_s}\right) \tag{A14}$$

Since $\mathbf{\Delta A_{11}} = \mathbf{\Delta A_{21}} = 0$, and using (A2) and (A4) in (A13) and (A14) yields

$$0 = \mathbf{A_{12}}\mathbf{e_\psi} + \beta\Delta\omega\mathbf{J}\hat{\boldsymbol{\psi}}_\mathbf{r} + \mathbf{K_1} sgn\left(\hat{\mathbf{I}}_\mathbf{s} - \mathbf{i_s}\right) \tag{A15}$$

$$\frac{d}{dt}\mathbf{e_\psi} = \mathbf{A_{22}}\mathbf{e_\psi} - \Delta\omega\mathbf{J}\hat{\boldsymbol{\psi}}_\mathbf{r} + \mathbf{K_2} sgn\left(\hat{\mathbf{I}}_\mathbf{s} - \mathbf{i_s}\right) \tag{A16}$$

Now, (A15) and (A16) can be rewritten using DQ coordinates as

$$\begin{bmatrix} 0 \\ 0 \end{bmatrix} = \beta \begin{bmatrix} \tau_r^{-1} & p\omega \\ -p\omega & \tau_r^{-1} \end{bmatrix} \begin{bmatrix} e_{D\psi} \\ e_{Q\psi} \end{bmatrix} + \beta \begin{bmatrix} 0 & -p\Delta\omega \\ p\Delta\omega & 0 \end{bmatrix} \begin{bmatrix} \hat{\psi}_{Dr} \\ \hat{\psi}_{Qr} \end{bmatrix} + \mathbf{K_1} sgn\left(\hat{\mathbf{I}}_\mathbf{s} - \mathbf{i_s}\right) \tag{A17}$$

$$\frac{d}{dt}\begin{bmatrix} e_{D\psi} \\ e_{Q\psi} \end{bmatrix} = \begin{bmatrix} -\tau_r^{-1} & -p\omega \\ p\omega & -\tau_r^{-1} \end{bmatrix} \begin{bmatrix} e_{D\psi} \\ e_{Q\psi} \end{bmatrix} - \begin{bmatrix} 0 & -p\Delta\omega \\ p\Delta\omega & 0 \end{bmatrix} \begin{bmatrix} \hat{\psi}_{Dr} \\ \hat{\psi}_{Qr} \end{bmatrix} + \mathbf{K_2} sgn\left(\hat{\mathbf{I}}_\mathbf{s} - \mathbf{i_s}\right) \tag{A18}$$

Expanding (A17) and (A18) gives

$$0 = \beta\tau_r^{-1} e_{D\psi} + \beta p\omega e_{Q\psi} - \beta p\Delta\omega\hat{\psi}_{Qr} + k_{11} sgn\left(\hat{\imath}_{Ds} - i_{Ds}\right), \tag{A19}$$

$$0 = -\beta p\omega e_{D\psi} + \beta\tau_r^{-1} e_{Q\psi} + \beta p\Delta\omega\hat{\psi}_{Dr} + k_{11} sgn\left(\hat{\imath}_{Qs} - i_{Qs}\right) \tag{A20}$$

$$\frac{de_{D\psi}}{dt} = -\tau_r^{-1} e_{D\psi} - p\omega e_{D\psi} + p\Delta\omega\hat{\psi}_{Qr} + k_{22} sgn\left(\hat{\imath}_{Ds} - i_{Ds}\right), \tag{A21}$$

$$\frac{de_{Q\psi}}{dt} = p\omega e_{D\psi} - \tau_r^{-1} e_{Q\psi} - p\Delta\omega\hat{\psi}_{Dr} + k_{22} sgn\left(\hat{\imath}_{Qs} - i_{Qs}\right). \tag{A22}$$

Dividing expressions (A19) and (A20) by β, and summing them with (A21) and (A22) yields

$$\frac{de_{D\psi}}{dt} = \left(\frac{k_{11}}{\beta} + k_{22}\right) sgn\left(\hat{\imath}_{Ds} - i_{Ds}\right), \tag{A23}$$

$$\frac{de_{Q\psi}}{dt} = \left(\frac{k_{11}}{\beta} + k_{22}\right) sgn\left(\hat{\imath}_{Qs} - i_{Qs}\right). \tag{A24}$$

Therefore, one verifies that (A23) and (A24) can be rewritten as

$$\frac{d}{d}\begin{bmatrix} e_{D\psi} \\ e_{Q\psi} \end{bmatrix} = \left(\frac{\mathbf{K_1}}{\beta} + \mathbf{K_2}\right) sgn\left(\hat{\mathbf{I}}_\mathbf{s} - \mathbf{i_s}\right). \tag{A25}$$

Since $\mathbf{K_2} = -\mathbf{L}\mathbf{K_1}$, (A25) can be written as

$$\frac{d}{d}\begin{bmatrix} e_{D\psi} \\ e_{Q\psi} \end{bmatrix} = \left(\frac{\mathbf{I}}{\beta} - \mathbf{L}\right)\mathbf{K_1} sgn\left(\hat{\mathbf{I}}_\mathbf{s} - \mathbf{i_s}\right). \tag{A26}$$

Doing $\mathbf{\Lambda} = \mathbf{L} - \frac{\mathbf{I}}{\beta}$ and remembering that $\mathbf{e_\psi} = \begin{bmatrix} e_{D\psi} \\ e_{Q\psi} \end{bmatrix}$ in (45), the rotor flux error equation becomes given by

$$\frac{d\mathbf{e_\psi}}{dt} = -\mathbf{\Lambda K_1} sgn\left(\hat{\mathbf{I}}_\mathbf{s} - \mathbf{i_s}\right). \tag{A27}$$

REFERENCES

1. Tursini, M., R. Petrella, and F. Parasiliti, "Adaptive sliding-mode observer for speed-sensorless control of induction motors," *IEEE Transactions on Industry Applications*, Vol. 36, No. 5, 1380–1387, Sep/Oct. 2000.
2. Zhang, Y. and V. Utkin, "Sliding mode observers for electric machines-an overview," *IEEE 2002 28th Annual Conference of the Industrial Electronics Society, IECON 02*, Vol. 3, 1842–1847, Nov. 5–8, 2002.
3. Lascu, C. and G.-D. Andreescu, "Sliding-mode observer and improved integrator with DC-offset compensation for flux estimation in sensorless-controlled induction motors," *IEEE Transactions on Industrial Electronics*, Vol. 53, No. 3, 785–794, Jun. 2006.
4. Lascu, C., I. Boldea, and F. Blaabjerg, "Comparative study of adaptive and inherently sensorless observers for variable-speed induction-motor drives," *IEEE Transactions on Industrial Electronics*, Vol. 53, No. 1, 57–65, Feb. 2006.
5. Proca, A. B. and A. Keyhani, "Sliding-mode flux observer with online rotor parameter estimation for induction motors," *IEEE Transactions on Industrial Electronics*, Vol. 54, No. 2, 716–723, Apr. 2007.
6. Lubin, T., S. Mezani, and A. Rezzoug, "Improved analytical model for surface-mounted pm motors considering slotting effects and armature reaction," *Progress In Electromagnetics Research B*, Vol. 25, 293–314, 2010.
7. Lascu, C., I. Boldea, and F. Blaabjerg, "A class of speed-sensorless sliding-mode observers for high-performance induction motor drives," *IEEE Transactions on Industrial Electronics*, Vol. 56, No. 9, 3394–3403, Sep. 2009.
8. Sheng, Y. and V. Ajjarapu, "A speed-adaptive reduced-order observer for sensorless vector control of doubly fed induction generator-based variable-speed wind turbines," *IEEE Transactions on Energy Conversion*, Vol. 25, No. 3, 891–900, Sep. 2010.

9. Gadoue, S. M., D. Giaouris, and J. W. Finch, "MRAS sensorless vector control of an induction motor using new sliding-mode and fuzzy-logic adaptation mechanisms," *IEEE Transactions on Energy Conversion*, Vol. 25, No. 2, 394–402, Jun. 2010.
10. Hasan, S. and I. Husain, "A Luenberger-sliding mode observer for online parameter estimation and adaptation in high-performance induction motor drives," *IEEE Transactions on Industry Applications* , Vol. 45, No. 2, 772–781, Mar.–Apr. 2009.
11. Ghanes, M. and G. Zheng, "On sensorless induction motor drives: Sliding-mode observer and output feedback controller," *IEEE Transactions on Industrial Electronics*, Vol. 56, No. 9, 3404–3413, Sep. 2009.
12. Hadef, M., M. R. Mekideche, A. Djerdir, and A. Miraoui, "An inverse problem approach for parameter estimation of interior permanent magnet synchronous motor," *Progress In Electromagnetics Research B*, Vol. 31, 15–28, 2011.
13. Lascu, C. and G.-D. Andreescu, "Sliding-mode observer and improved integrator with DC-offset compensation for flux estimation in sensorless-controlled induction motors," *IEEE Transactions on Industrial Electronics*, Vol. 53, No. 3, 785–794, Jun. 2006.
14. Foo, G. H. B. and M. F. Rahman, "Direct torque control of an IPM-synchronous motor drive at very low speed using a sliding-mode stator flux observer," *IEEE Transactions on Power Electronics*, Vol. 25, No. 4, 933–942, Apr. 2010.
15. Iqbal, M., A. I. Bhatti, S. I. Ayubi, and Q. Khan, "Robust parameter estimation of nonlinear systems using sliding-mode differentiator observer," *IEEE Transactions on Industrial Electronics*, Vol. 58, No. 2, 680–689, Feb. 2011.
16. Foo, G. H. B. and M. F. Rahman, "Direct torque control of an ipm-synchronous motor drive at very low speed using a sliding-mode stator flux observer," *IEEE Transactions on Power Electronics*, Vol. 25, No. 4, 933–942, Apr. 2010.
17. Kim IL-S., "A technique for estimating the state of health of lithium batteries through a dual-sliding-mode observer," *IEEE Transactions on Power Electronics*, Vol. 25, No. 4, 1013–1022, Apr. 2010.
18. Hasan, S. and I. Husain, "A Luenberger-sliding mode observer for online parameter estimation and adaptation in high-performance induction motor drives," *IEEE Transactions on Industry Applications*, Vol. 45, No. 2, 772–781, Mar.–Apr. 2009.

19. Ghanes, M., J. de Leon, and A. Glumineau, "Cascade and high-gain observers comparison for sensorless closed-loop induction motor control," *Control Theory & Applications, IET*, Vol. 2, No. 2, 133–150, Feb. 2008.
20. Mahmoudi, A., N. A. Rahim, and H. W. Ping, "Genetic algorithm and finite element analysis for optimum design of slotted torus axial-flux permanent-magnet brushless DC motor," *Progress In Electromagnetics Research B*, Vol. 33, 383–407, 2011.